

# Resistivity and Tunnel Magnetoresistance in Double-Perovskite Strontium Ferromolybdate Ceramics

Gunnar Suchaneck,\* Evgenii Artiukh, and Gerald Gerlach

The low-field magnetoresistance properties in double-perovskite strontium ferromolybdate core-shell structures arise from spin-dependent tunneling through a barrier formed by the shell. It is strongly dependent on synthesis conditions. In this work, first, the resistivity behavior of granular strontium ferromolybdate ceramics comprising intergrain tunnel barriers is reviewed. Based on this generalization, the modification of the tunneling process with barrier thickness and interface conditions is demonstrated. For the first time, equations for the magnetoresistance in each special case are derived.

## 1. Introduction

Magnetoresistance (MR) is the property of a material to change the value of its electrical resistance in an externally applied magnetic field. The intrinsic MR of a material is then defined by

$$\text{MR} = \frac{\rho(B) - \rho(0)}{\rho(0)} \quad (1)$$

where  $\rho$  is the resistivity and  $B$  is a given magnetic flux density.

The magnetoresistive effects in materials are classified into several categories according to their driving mechanisms, namely the anisotropic magnetoresistance (AMR) first observed by Lord Kelvin in 1857 in nickel and iron.<sup>[1]</sup> Here, the electrical resistivity depends on the relative angle between the magnetization direction and the electric current direction. The electrical resistance has its maximum value when the direction of current is parallel to the applied magnetic field. To obtain a linear sensor characteristic, the current path should be 45° inclined to the

anisotropy axis. This is realized by a so-called barber-pole configuration, which consists of metal stripes placed on a thin film of permalloy inclined at an angle of 45°. The giant magnetoresistance (GMR) awarded by the Nobel prize to Albert Fert and Peter Grünberg in 2007, representing a quantum mechanical magnetoresistance effect changing the direction of magnetization of the adjacent ferromagnetic layer which was observed in multilayers composed of alternating ferromagnetic and nonmagnetic conductive layers<sup>[2,3]</sup> as well

as in granular single-domain Co particles embedded in a Cu medium.<sup>[4,5]</sup> The tunnel magnetoresistance (TMR), a magnetoresistive effect, that occurs in a magnetic tunnel junction consisting of two ferromagnets separated by a thin insulator.<sup>[6]</sup> The colossal magnetoresistance (CMR), a property of some materials, mostly manganese-based perovskite oxides, that enables them to dramatically change their electrical resistance in the presence of a magnetic field,<sup>[7,8]</sup> and the extraordinary magnetoresistance (EMR), a geometrical magnetoresistance effect, occurring in semiconductor-metal hybrid systems when a transverse magnetic field is applied.<sup>[9,10]</sup>

Table 1 compiles the main characteristics of these various magnetoresistive effects at room temperature. The comparison shows that even the TMR is beneficial for application due to its high MR value. Additionally, high-resistance and low-resistance sensors might be fabricated with the same design just by changing the barrier thickness in the TMR deposition process. This enables adapting impedance to a certain application. However, the increase of thermal noise by high sensor resistance should be taken into account. The large temperature coefficient of resistance of CMR materials close to the insulator-metal transition temperature makes them suitable for bolometer applications.<sup>[11]</sup>

Since the electrical conduction and magnetization of strontium ferromolybdate (SFMO) are very sensitive to sample preparation also other mechanisms of MR become possible: A first mechanism is the intragrain tunneling resistance across antiphase boundaries.<sup>[12]</sup> In SFMO ceramics, antiphase boundaries remain as relicts of grain boundaries after prolonged annealing at intermediate temperatures around 900 °C.<sup>[13]</sup> A magnetoresistance attributed to the tunneling across antiphase boundaries was obtained in epitaxial SFMO films grown by pulsed laser deposition in an oxidizing atmosphere.<sup>[14]</sup> Another mechanism in double perovskite in half-metallic double-perovskite Sr<sub>2</sub>CrWO<sub>6</sub> thin films is that an external magnetic field suppresses the long-range antiferromagnetic order to form short-range antiferromagnetic fluctuations, which enhance electronic scattering and lead to the giant positive MR.<sup>[15]</sup> A third possible mechanism is related to a

G. Suchaneck, G. Gerlach  
Solid State Electronics Laboratory  
TU Dresden  
01062 Dresden, Germany  
E-mail: gunnar.suchaneck@tu-dresden.de

E. Artiukh  
Cryogenic Research Division  
SSPA "Scientific-Practical Materials Research Centre of NAS of Belarus"  
220072 Minsk, Belarus

 The ORCID identification number(s) for the author(s) of this article can be found under <https://doi.org/10.1002/pssb.202200012>.

© 2022 The Authors. physica status solidi (b) basic solid state physics published by Wiley-VCH GmbH. This is an open access article under the terms of the Creative Commons Attribution License, which permits use, distribution and reproduction in any medium, provided the original work is properly cited.

DOI: 10.1002/pssb.202200012

**Table 1.** Comparison of the characteristics of magnetoresistive effects.

Magnetoresistive effect	AMR	GMR	TMR	CMR	EMR
Maximum value of MR [%]	1–3	10–20	20–200	20–100	$10^3$ – $10^4$
Field range [T]	$10^{-10}$ – $10^{-2}$	$10^{-10}$ – $10^4$	$10^{-11}$ – $10^{-2}$	$10^{-3}$	0.5–3
Resistance [k $\Omega$ ]	$\approx 1$	5–30	$0.01$ – $10^4$	0.1–100	$10^{-5}$ – $10^{-3}$
Temperature coefficient of resistance [%]	0.2–0.3	0.05–0.1	0.1–0.2	2–10	0.2–1.0

metallic–insulator transition in perovskite oxides.<sup>[16]</sup> Sr substitution by Ba in  $\text{Sr}_{2-x}\text{Ba}_x\text{FeMoO}_{6-\delta}$  leads to a transition from metallic behavior at  $x \leq 1.6$  to an insulating behavior at  $x \geq 1.7$  attributed to a valence transition of  $\text{Fe}^{3+}$  ion to the  $\text{Fe}^{2+}$  state.<sup>[17]</sup> This induces a localization of the itinerant electrons and an insulating behavior of the compounds. The low-field magnetoresistance (LFMR) is enhanced substantially as  $x$  increases for  $0 < x \leq 0.4$ , decreases gradually for  $0.4 < x \leq 1.6$ , and drops to a very small value for  $x \geq 1.7$ . A metal–semiconductor transition occurs in ordered double-perovskite oxides  $\text{Sr}_2\text{Fe}_x\text{Mo}_{2-x}\text{O}_6$  ( $0.8 \leq x \leq 1.5$ ).<sup>[18]</sup> Samples with  $x \geq 1.2$  are semiconducting in the temperature range of  $4 \leq T \leq 300$  K. A semiconductor–metal transition occurs in samples with  $x < 1.2$  as temperature increases and the semiconductor–metal transition temperature decreases rapidly as Fe content decreases. Two metal–insulator transitions were found between 300 and 900 K in SFMO ceramics at  $T_1 \approx 405$  K near to the Curie temperature and  $T_2 \approx 590$  K.<sup>[19]</sup> Below the first transition, the material is metallic and magnetically ordered. Above 590 K, it shows a metallic behavior again, while in the range  $405 \text{ K} < T < 590 \text{ K}$ , a weak localization was observed.

In this work, we focus on the TMR effect. In magnetic materials, this is the most sensitive MR effect at room temperature (cf. Table 1). The first report<sup>[6]</sup> demonstrated a relative resistance change of around 14% in Fe/Ge–O/Co–junctions at 4.2 K. Sizable room temperature values of 11.8% in CoFe/Al<sub>2</sub>O<sub>3</sub>/Co junctions and 18% in Fe/Al<sub>2</sub>O<sub>3</sub>/Fe junctions were first reported in 1995 by Moodera<sup>[20]</sup> and Miyazaki,<sup>[21]</sup> respectively. Theoretically, values up to 1000% were predicted in Fe/MgO/Fe structures.<sup>[22,23]</sup> Experimentally, TMR values of up to 604% at room temperature were observed in CoFeB/MgO/CoFeB junctions.<sup>[24]</sup> TMR sensors cover a resistance range from a few Ohm to some MOhm. High resistance as well as low-resistance sensor might be built by the same design just by changing the barrier thickness.<sup>[25]</sup>

Oxide perovskites with ferromagnetic behavior around room temperature were first reported in the 1950s in the pioneering studies on manganites.<sup>[7]</sup> In polycrystalline lanthanum strontium manganite ceramics, an extrinsic LFMR was found in 1996.<sup>[26]</sup> It was shown that the magnetoresistance in polycrystalline lanthanum strontium manganite exhibits two distinct regions: 1) large magnetoresistance at low fields dominated by spin-dependent tunneling between grains; and 2) high-field magnetoresistance obtained also in single crystals. The discovery of LFMR and half-metallicity of the SFMO by Kobayashi et al. in 1998<sup>[27]</sup> renewed the interest in these materials in the context of their potential applications in the field of spin electronics.

In this work, we review first the resistivity behavior of granular SFMO ceramics comprising intergrain tunnel barriers.

Based on this generalization, we illustrate the modification of the tunneling process with barrier thickness and interface conditions. We derive equations for the MR in each special case for the first time.

The remainder of this paper is organized as follows: In Section 2, we consider the intrinsic resistivity of SFMO as well as the most common models of tunnel resistance applied to SFMO. The following, main Section 3 discusses the magnetoresistance based on the already described tunnel resistance models. It starts with the examination of the magnetic field dependence of the tunneling barrier parameters and afterward considers the dominating intergrain conductivity mechanisms depending on the film thickness. Conclusions are presented in Section 4.

## 2. Resistivity

### 2.1. Intrinsic Resistivity

SFMO shows a tetragonal structure with the  $I4/m$  space group<sup>[28]</sup> though some authors believe its space group to be  $I4/mmm$  with a lowered symmetry.<sup>[29–31]</sup> The perfect SFMO lattice structure is built up by ordering FeO<sub>6</sub> and MoO<sub>6</sub> oxygen octahedra in a rock salt lattice while the Sr cations are in the cubic octahedral voids formed by the octahedral. SFMO presents half-metallic character consisting of two conduction channels, that is, the material is a semiconductor for the up-spin band, but is a metal for the down-spin band since the latter is continuous at the Fermi level.<sup>[27]</sup> In the following, we consider the metallic conductivity of the down-spin channel.

The temperature dependence of the resistivity of SFMO single crystals is described by<sup>[32–34]</sup>

$$\rho_i(T) = \rho_0 + R_2 T^2 \quad (2)$$

with a residual resistivity  $\rho_0$  and a coefficient  $R_2 = 2.5 \times 10^{-10} \Omega \text{ m K}^{-2}$ , suggesting that either electron–electron scattering or spin–wave scattering dominates the resistivity. In SFMO, the conduction electron density has Mo 4d character,<sup>[35]</sup> and, hence, the cross section of electron–electron interactions will be small.<sup>[36]</sup> An alternative origin of the observed  $T^2$ -dependence is scattering of long wavelength spin waves in ferromagnetic metals.<sup>[37]</sup> In our case, conduction electrons should be scattered by the localized core spins of the  $\text{Fe}^{3+}$  ( $S = 5/2$ ) ions. However, the estimated temperature coefficient  $R_2 \approx 2 \times 10^{-14} \Omega \text{ m K}^{-2}$  is about four orders of magnitude lower than the experimental one. One reason for this could be the incorrect consideration of the  $s$ - $d$  interaction in a ferromagnetic half-metal with low-electron concentration at the Fermi

level<sup>[32,34,38]</sup> and with full spin subband splitting.<sup>[27]</sup> In contrast, spin-wave scattering is expected to be suppressed in half-metal SFMO by a factor of  $\exp(-\delta/kT)$  with  $\delta$  being the gap between the majority and minority spin levels<sup>[39]</sup> ( $\delta = 0.7 \dots 0.8 \text{ eV}$ <sup>[27,40]</sup>) because of the majority spin-band will be not populated at low temperatures. The minimum of conductivity observed in SFMO ceramics at low temperatures is decreasing with magnetic flux density from about 150 K at  $B = 0.2 \text{ T}$  to about 40 K at  $B = 7 \text{ T}$ .<sup>[27]</sup> With regard to Equation (2), it has extrinsic character, that is, it is attributed to the presence of grain boundaries.

In manganites  $\text{La}_{1-x}\text{A}_x\text{MnO}_3$  ( $A = \text{Sr, Ca, Pb}$ ) possessing half-metal character only at very low temperatures  $T/T_C < 0.2$  with  $T_C$  the Curie temperature,<sup>[41]</sup> the coefficient  $R_2$  shows a magnetic-field dependence at intermediate temperatures  $0.2 \leq T/T_C \leq 0.5$ , that is, in the region of ferromagnetic metal behavior.<sup>[41,42]</sup> This leads to a linear intrinsic magnetoresistance

$$\text{MR} = \frac{\left(\frac{\partial R_2}{\partial B}\right) T^2 \cdot B}{\rho_0 + R_2(0) T^2} \quad (3)$$

Assuming  $R_2(0) \approx 1.0 \times 10^{-10} \Omega \text{ m K}^{-2}$ ,  $\partial R_2/\partial B \approx 1.5 \times 10^{-12} \Omega \text{ m K}^{-2} \text{ T}^{-1}$ ,  $\rho_0 = 9.14 \times 10^{-7} \Omega \text{ m}$ ,<sup>[41]</sup> and  $B = 1 \text{ T}$ , the MR at 200 K amounts to 1.22%, that is, it can be neglected in the presence of other, more pronounced mechanisms of magnetoresistance.

The SFMO single-crystal data<sup>[32]</sup> is also well modeled by an alternative temperature dependence

$$\rho_i(T) = \rho_0 + R_{2.5} T^{2.5} \quad (4)$$

with a coefficient  $R_{2.5} = 1.4 \times 10^{-11} \Omega \text{ m K}^{-5/2}$ . The  $T^{5/2}$  law corresponds to the temperature dependence of the mean free path of spin-waves  $l_{\text{sw}}$  possessing a wave vector independent on temperature<sup>[43]</sup>

$$l_{\text{sw}} \approx 0.381 \cdot S^{9/2} a \cdot \left(\frac{J}{kT}\right)^{5/2} \quad (5)$$

where  $S$  is the effective spin,  $a$  is a quasi-cubic lattice parameter,  $J$  is the exchange integral between nearest neighbors amounting for SFMO to  $-4.1 \text{ meV}$ ,<sup>[32]</sup> and  $k$  is the Boltzmann constant. The temperature coefficient of the temperature-dependent part of the resistivity

$$\rho_{2.5}(T) = R_{2.5} T^{2.5} = \frac{\hbar k_F}{n_e e^2 l_{\text{sw}}} \quad (6)$$

was calculated assuming a Fermi surface of the itinerant  $d_i$  electrons approximated by a sphere of radius of the Fermi wave vector  $k_F = (3\pi n_e)^{1/3}$  where  $n_e \approx 1 \times 10^{28} \text{ m}^{-3}$ <sup>[32,34,38]</sup> is the electron density,  $e$  is the electron charge, and  $\hbar$  is the Planck constant expressed in  $\text{J s radian}^{-1}$ . This yields  $R_{2.5} \approx 3 \times 10^{-10} \Omega \text{ m K}^{-5/2}$ , that is, the coefficient is overestimated by about one order of magnitude. Thereby, a factor of two is at least related to the approximation of the Fermi surface as a sphere.<sup>[44]</sup> Another reason for the overestimation of  $R_2$  might be the neglect of additional  $s$ - $d$  transitions in transition metals in ref. [43], which further reduce the mean free path.

In general, the intrinsic resistivity of SFMO can be modeled by a relation

$$\rho_i(T) = \rho_0 + R_\nu T^\nu \quad (7)$$

where  $\nu$  is a fitting parameter in the order of 2.5.

The residual, metallic resistivity of SFMO grain is often described by means of the Drude model

$$\rho_D = \frac{\hbar k_F}{n_e e^2 l_e} \quad (8)$$

where  $l_e$  is the electron mean free path. If  $n_e$  is proportional to the density of states  $n(E_F)$  at Fermi level  $E_F$ , the resistivity near a temperature of 0 K is given by<sup>[45]</sup>

$$\rho_D = [e^2 n(E_F) v_F^2 \tau]^{-1} \quad (9)$$

where  $v_F = l_e/\tau$  is the Fermi velocity and  $\tau^{-1}$  is the electron-scattering rate. Since  $n(E_F)$  increases upon a rise of the superstructural ordering degree of the Fe/Mo cations, while  $v_F$  and  $\tau$  at a fixed temperature are constant, a rise of  $n(E_F)$  causes a reduction of  $\rho$ .<sup>[46]</sup> Note that Equation (9) overestimates  $n(E_F)$  in SFMO by about 50% because of the made simplifications.

Calculations of  $\rho_D$  by means of Equation (8) were carried out assuming  $n_e = 1.1 \cdot 10^{22} \text{ cm}^{-3}$ <sup>[32]</sup> and  $l_e(4 \text{ K}) = 1.11 \text{ nm}$ <sup>[47]</sup> yielding a value of  $\rho_0 \approx 2 \times 10^{-6} \Omega \text{ m}$  in good agreement with the obtained one, of  $\rho = 1.8 \times 10^{-6} \Omega \text{ m}$  in single-crystal SFMO at 4 K.<sup>[34]</sup> Note that the electron mean free path at low temperatures exceeds the atomic dimension by about a factor of three. Consequently, we have to deal rather with delocalized electrons than electrons hopping between localized sites. This corresponds to a conduction process mediated by delocalized Mo electrons.<sup>[48]</sup> However, following a recent report,<sup>[49]</sup> the conductivity picture should be more complex because of strong indirect Fe-O-Mo hopping.

## 2.2. Tunneling Resistance

### 2.2.1. Tunneling Resistance Across Intergrain Barriers

Since the spin-up states have an energy gap at the Fermi level, intergrain tunneling occurs between the spin-down states of SFMO grains. The tunneling process is illustrated in **Figure 1**.

The electron conduction in polycrystalline, granular SFMO is dominated by the electron transfer through the grain boundaries between conducting grains. In contrast, the resistivity of a granular metal network in which the metal grains are interconnected by insulating barriers is given by<sup>[50]</sup>

$$\rho_T(T) \propto \exp\left(f\chi w + \frac{U_c}{2kT}\right) \quad (10)$$

where  $f$  is a shape factor that amounts to 2 for a rectangular barrier and to  $\pi/2$  for a parabolic barrier.  $\chi$  is the reciprocal localization length of the wave function

$$\chi = \sqrt{\frac{2m^*\Phi}{\hbar^2}} \quad (11)$$

where  $m^*$  is the effective electron mass,  $\Phi$  is the barrier height,  $w$  is the barrier width, and  $U_c$  is the charging energy of the grains. Here, we consider thin enough barriers in the order of

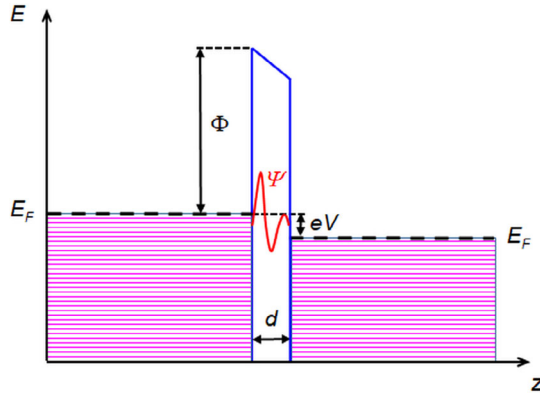


**Figure 1.** Electron tunneling between two strontium ferromolybdate (SFMO) grains biased by a voltage  $V$  through a barrier with barrier height  $\Phi$ . Illustrated are the spin-down states which are filled up to the Fermi level  $E_F$ . Also shown is the exponential damping of a wave function  $\Psi$  within a 1D potential barrier.

1–3 nm where direct tunneling occurs which is not disturbed by localized states in the thin barrier film.<sup>[51]</sup> An estimation of  $U_c$  for a grain of diameter  $d$  with  $d \gg w$  is given by<sup>[52]</sup>

$$U_c \approx \frac{4e^2}{\epsilon\epsilon_0 d} \cdot \frac{w}{d} \quad (12)$$

where  $\epsilon$  is the dielectric constant, and  $\epsilon_0$  is the vacuum permittivity. Since the charging energy is reciprocal to the grain diameter  $d$ , charging effects become significant at small grain sizes. In a case of nanosized, granular SFMO with  $d = 75$  nm and  $w = 1.24$  nm,<sup>[53]</sup>  $U_c$  yields a value of  $U_c \approx 0.8$  meV for  $\epsilon \approx 20$  that is in good agreement with data of mechanically ball-milled SFMO<sup>[54]</sup> possessing a similar grain size.<sup>[55]</sup> Thus,  $U_c$  is negligible in this case.

Tunneling proceeds by the simultaneous tunneling of a charge carrier from one grain serving as electrode via other grains to another electrode. Tunneling itself is a temperature-independent transport process.<sup>[56]</sup>

In the following, we consider a tunneling process between magnetic grain in a granular structure. Spin-dependent electron tunneling depends on the relative orientation of magnetic moments between the ferrimagnetic grains of SFMO. The tunnel resistance decreases when the magnetic moments of the grains are aligned in parallel in an applied magnetic field. If the angle between the magnetizations on both sides of the tunneling barrier is randomly distributed between 0 and  $\pi$ , then the resistivity is given by<sup>[57]</sup>

$$\rho_T(T) = \frac{\rho_i(T) \cdot \exp(f\chi w)}{1 + m^2(B, T) \cdot P^2} \quad (13)$$

where  $m$  is the relative magnetization, that is, the magnetization  $M$  is scaled to the saturation magnetization  $M_s$ , and  $P$  is the spin polarization in the magnetic grains.

In many reports investigating granular systems<sup>[50,52,57–59]</sup> including also SFMO,<sup>[54,60]</sup> the argument of the exponent in Equation (10) is summed up in one parameter, for example,

$\Delta$ , being proportional to the composition and thickness of the tunneling barrier.

### 2.2.2. Tunneling Resistance in the Presence of a Magnetically Disordered Interface Layer

In a transport process, where the electron first moves from the bulk of a first grain to a state in a disordered interface layer and then into the bulk of a second grain, the conductivity across a grain boundary is determined by the spin orientation both in the two grains and in the disordered interface layer. When the bulk magnetization  $\mathbf{M}$  is saturated, the spins in the grains become parallel. The conductivity assuming randomly disordered spins in the interface layer is then given by<sup>[61]</sup>

$$\frac{\Delta\sigma}{\sigma(0)} \propto 1 + \langle (\mathbf{M} \cdot \mathbf{S}_b)^2 \rangle \quad (14)$$

where  $\sigma(0)$  is the zero-field conductivity and  $\mathbf{S}_b$  is the spin direction in the interface layer. The second term can be written as  $M^2 \langle \cos^2 \theta \rangle$  yielding  $M^2/3$ . Correspondingly, we rewrite Equation (13) as

$$\rho_T(T) = \frac{\rho_i(T) \cdot \exp(f\chi w)}{1 + 1/3 \cdot m^2(B, T) \cdot P^2} \quad (15)$$

### 2.2.3. Tunneling Resistance Beyond Thin-Barrier Limit

Beyond the thin-barrier limit, intergrain resistivity of granular materials is determined by inelastic hopping via localized states within the barrier.<sup>[51]</sup> Here, the temperature dependence of the spin-independent, higher-order tunneling conductance is given by

$$\sigma_{ih} \propto T^\nu, \nu = n - [2/(n+1)] \quad (16)$$

where  $n$  is the number of localized states in the hopping channel.

The lowest-order hopping channel via two localized states ( $n = 2$ ) exhibits an electrical conductivity term  $G_{4/3} \cdot T^{4/3}$ , where the temperature coefficient  $G_{4/3}$  yields

$$G_{4/3} = \nu_{2,T} \cdot \frac{e^2}{\hbar^2} \cdot \frac{n(E_F)^2 k^{4/3} \Lambda^{2/3} U_0^{4/3} w^2}{\chi^3 \rho^{1/3} v_s^{5/3}} \cdot \exp\left(-\frac{f\chi w}{3}\right) \quad (17)$$

The value  $\nu_{2,T} = 50$  is a numerical coefficient,  $\Lambda$  the average deformation potential,  $U_0$  is the binding energy of localized states with

$$U_0 = \frac{\pi^2 \hbar^2}{2m^* w^2} \quad (18)$$

$\rho$  is the density of tetragonal SrMoO<sub>4</sub> (SMO, space group  $I4_1/a$ ) as the barrier material, and  $v_s$  the average sound velocity. A crude estimation of  $G_{4/3}$  using the data compiled in the Supporting Information yields a value of  $4.71 \times 10^{-4} \Omega^{-1} \text{cm}^{-1} \text{K}^{-4/3}$  in satisfactory agreement with coefficients experimentally obtained in SFMO.<sup>[54,60]</sup> Following Equation (16), inelastic hopping through the tunneling barrier leads to a conductivity contribution represented by<sup>[62]</sup>

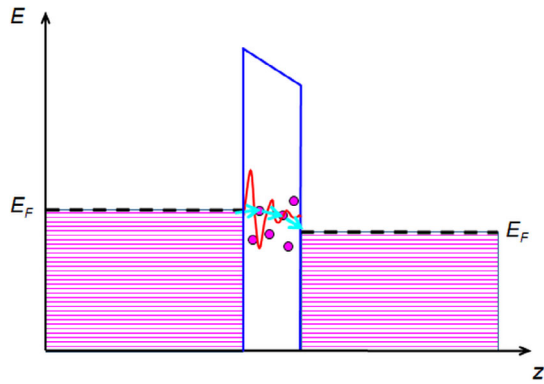


**Figure 2.** Parallel electron tunneling and inelastic hopping through SFMO–dielectric barrier–SFMO junctions.

$$\sigma_{\text{ih}}(T) = G_{4/3}T^{4/3} + G_{5/2}T^{5/2} + G_{18/5}T^{18/5} + \dots \quad (19)$$

A process of parallel tunneling and inelastic hopping via localized states is shown schematically in **Figure 2**.

**Figure 3** illustrates the evolution of the resistivity behavior of nanosized ( $d \approx 75$  nm) SFMO ceramics synthesized by means of the citrate gel technique including a final annealing in a reducing environment of a 5% $\text{H}_2$ /Ar gas mixture at 900 °C for 4 h.<sup>[53]</sup> The samples were first pressed into tablets with a diameter of 10 mm and a thickness of 3 mm under a pressure of 4 GPa at 530 °C for 1 min—sample SFMO I. The resistivity of this sample is well described by Equation (13) including Equation (7) with  $\nu = 2.62$ —model I.

After post-annealing for 3 h in an Ar flow (99.998%,  $p_{\text{O}_2} \leq 0.25$  Pa) sample—SFMO II, the resistivity is determined by two parallel conduction channels, one occurring also in sample SFMO-I, but possessing a larger barrier width, the other following Equation (19) with  $G_{4/3} = 2.7 \times 10^{-4} \Omega^{-1} \text{cm}^{-1} \text{K}^{-4/3}$  derived from Equation (17) and  $G_{5/2} \approx 7.5 \times 10^{-7} \Omega^{-1} \text{cm}^{-1} \text{K}^{-5/2}$  determined by curve fitting with model II

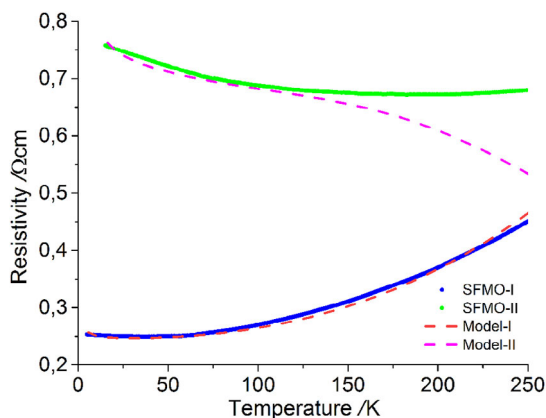


**Figure 3.** Comparison of the resistivity of an nanosized SFMO sample as-fabricated by the citrate–gel technique<sup>[53]</sup> with model I, Equations (7) and (13), and an post-annealed SFMO sample with model II, Equation (20).

$$\rho_{\text{T+ih}}(T) = \left[ \frac{1}{\rho_{\text{T}}(T)} + \sigma_{\text{ih}}(T) \right]^{-1} \quad (20)$$

To improve fitting at low temperatures, a factor  $\exp(U_c/2kT)$  was added in the following equation, Equation (10). The corresponding charging energies  $U_c$  were estimated as 0.05 and 0.19 meV for samples SFMO-I and SFMO-II, respectively. In the case of sample SFMO-II, the fit may be further improved by consideration of higher order terms in Equation (19). This reduces the coefficient  $G_{5/2}$  which is obviously overestimated in our case, but is already in the order of a value given in literature.<sup>[60]</sup> Nevertheless, the available experimental data does not allow the derivation of reliable higher-order coefficients.

Further annealing up to 5 h leads to the fluctuation-induced tunneling (FIT) at low temperatures and Mott variable range hopping near room temperature considered before (cf. ref. [53]). Mott variable range hopping represents the high-temperature and thick-barrier limit of inelastic hopping.<sup>[51]</sup>

#### 2.2.4. Tunnel Resistance Across Intergrain Nanocontacts

Let us now consider cold-pressed or low-temperature-annealed SFMO comprising nanocontacts, for example, via conducting paths in a dielectric intergrain barrier between metallic grains which form a capacitance  $C$  at the interface. The corresponding charge-carrier transport is depicted in **Figure 4**. In such a system, thermal fluctuations occur when the electrostatic energy per electron,  $e^2/2C$ , is much smaller than the thermal one,  $kT/2$ , with  $e$  the electron charge and  $k$  the Boltzmann constant. The random mean square noise voltage generated on an ideal capacitor in an RC circuit is then given by  $(kT/C)^{1/2}$ .<sup>[63]</sup> For a dielectric constant of 20, a barrier width  $w$  of 2 nm, and a contact area  $A$  of 1000 nm<sup>2</sup>, the junction capacitance  $C$  will be in the order of 0.1 fF. This yields a ratio  $e^2/(CkT)$  in the order of 0.1 in the temperature region 50–300 K.

Conducting grains separated by energy barriers subjected to large thermal fluctuations are modeled by the FIT model.<sup>[64]</sup> The FIT model links the temperature-independent tunneling conductivity<sup>[56]</sup> with a temperature-dependent conductivity obtained for tunneling of spin-polarized electrons in granular metal films.<sup>[50]</sup> It is specified by two parameters: 1) the

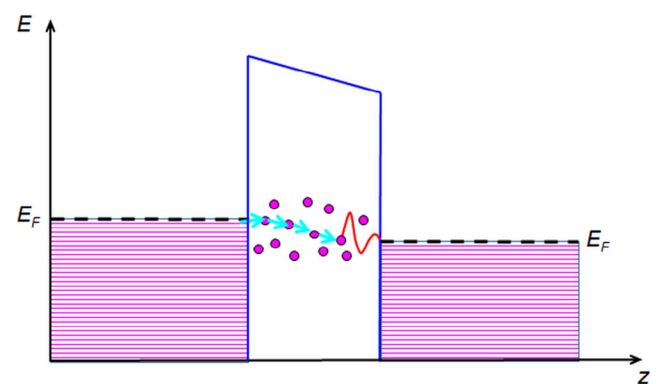


**Figure 4.** Charge-carrier hopping via localized states in a dielectric barrier between conducting grains to a tunneling site near a nanocontact.

temperature  $T_1$  characterizing the electrostatic energy of a parabolic potential barrier

$$kT_1 = \frac{A \cdot w \cdot \epsilon_0 E_0^2}{2} \quad (21)$$

where  $\epsilon_0$  is the vacuum permittivity and  $E_0$  is the characteristic field determined by the barrier height  $\Phi$

$$E_0 = \frac{4\Phi}{e \cdot w} \quad (22)$$

and 2) the temperature  $T_0$  representing  $T_1$  divided by the tunneling constant

$$T_0 = T_1 \cdot \left(\frac{f\chi w}{2}\right)^{-1} \quad (23)$$

The resistivity resulting by this model yields

$$\rho(T) = \rho_0 \exp\left(\frac{T_1}{T_0 + T}\right) \quad (24)$$

that is, the samples possess a resistivity decreasing with temperature.<sup>[53,65–69]</sup> At  $T \ll T_0$ , that is, for large electrostatic energy, the conductivity is temperature independent and corresponds to the expected formula for tunneling through a parabolic barrier. However, at high temperatures  $T$  is much larger than  $T_0$ , that is, for small electrostatic energy, the behavior becomes that of thermal activation.

## 3. Magnetoresistance

### 3.1. Magnetic-Field Dependence of the Tunneling Barrier

In nanosized, granular SFMO–SMO core-shell structures, the barrier thickness is in the order of  $w \approx 1/\chi$ .<sup>[53]</sup> In contrast, the barrier is much thinner than the magnetic length  $l_B = (\hbar/eB)^{1/2}$ . In this case, the barrier height was experimentally found to follow the series expansion<sup>[70]</sup>

$$\Phi(B) = \Phi_0(0) - \beta B + \gamma B^2 \quad (25)$$

The barrier height was taken as the hopping barrier between nearest neighbor (Fe–Mo) sites,  $\Phi_0 = 0.27$  eV.<sup>[71]</sup> The coefficient  $\beta$  was attributed to Zeeman splitting amounting to about  $1\mu_B$  ( $1\mu_B \approx 0.058$  meV T<sup>-1</sup>) for a magnetic field perpendicular and about  $18\mu_B$  for a magnetic field applied parallel to the current.<sup>[70]</sup> In our case, the coefficient  $\beta$  was chosen as  $\beta = 20\mu_B$ . The out-of-plane coefficient  $\gamma$  was adapted from data of a magnetic sensor based on a Pt/La<sub>2</sub>Co<sub>0.8</sub>Mn<sub>1.2</sub>O<sub>6</sub>/SrTiO<sub>3</sub>:Nb tunneling device with a 2 nm thick tunnel barrier<sup>[70]</sup> yielding  $\gamma = 0.034$  meV T<sup>-2</sup>. A theoretical estimate of  $\gamma$  is given by<sup>[72]</sup>

$$\gamma = \frac{z^2 e^2 B^2}{6m^*} \quad (26)$$

Assuming an effective value of  $z$  to be  $z_{\text{eff}} = (\pi/4)^{1/2}d$  with  $d = 75$  nm,<sup>[53]</sup> we obtain  $\gamma = 0.052$  meV T<sup>-2</sup> for  $m^* = 2.5m_e$ . Consequently, we have fixed the value of  $\gamma$  to  $0.040$  meV T<sup>-2</sup> providing the best fit to of the experimental data.

### 3.2. Tunnel Magnetoresistance

#### 3.2.1. Intergrain MR Due to Spin-Dependent Tunneling

The main contribution to the technologically important LFMR in SFMO arises from spin-dependent electron tunneling across insulating grain boundaries. Three models are applied for the description of MR: the empirical exponential model<sup>[68]</sup> is simply a good approximation of the experimental results for both sintered and granular SFMO ceramic samples. The tunneling model developed for barium–strontium ferromolybdate<sup>[73]</sup> considers the conductivity due to elastic direct tunneling occurring through a barrier 1) between two noninteracting grains; 2) equal spin polarization  $P$  but different directions in the neighboring grains, under an external magnetic field  $H$ . The modified tunneling model,<sup>[74]</sup> improving the fit to the LFMR data by adding an empirical tanh-function correction at low fields.

The average cosine of the angle between the magnetization directions of two neighboring grains yields the squared reduced magnetization,  $m^2$ .<sup>[73,75]</sup> The resulting magnetoconductivity is then given by

$$\frac{\Delta\sigma}{\sigma_0} = m^2 P^2 \quad (27)$$

In contrast, the grain surface is a defective double perovskite, where off-stoichiometry, vacancies, and antisite disorder (ASD) act as random spin pinning centers. This suppresses ferromagnetism. Therefore, the bulk-reduced magnetization was replaced in ref. [73] by a magnetic-field-dependent, reduced magnetization  $m_{\text{gb}}$  of the region close to the grain boundary, which was taken in a functional form widely used in spin glasses possessing a weak anisotropy field

$$m(B) = m_{\text{gb}}(B) = \left[1 - \left(\frac{B_{\text{cr}}}{B}\right)^{1/2}\right] \quad (28)$$

Here,  $B_{\text{cr}}$  was taken as an empirical parameter describing some critical magnetic flux density. Rewriting Equation (27) in terms of magnetoresistivity, we arrive at<sup>[73]</sup>

$$\frac{\Delta\rho}{\rho_0} = \frac{m^2 P^2}{1 + m^2 P^2} - bB \quad (29)$$

where the intragrain MR is accounted by adding a linear term  $bB$ . This term is typically large near the magnetic ordering temperature. We neglect it in the further considerations. For the limit of a large magnetic flux density compared to the critical one,  $B \gg B_{\text{cr}}$ , the empirical model<sup>[68]</sup>

$$\frac{\Delta\sigma}{\sigma_0} \propto \exp\left[-\left(\frac{B_{\text{cr}}}{B}\right)^{1/2}\right] \quad (30)$$

coincides with the tunneling one.<sup>[73]</sup> To improve the fit to the MR data of pressed for barium–strontium ferromolybdate powders at low fields, an empirical hyperbolic tangent function correction was added later<sup>[74]</sup>

$$m_{\text{gb}}(B) = c \cdot \tanh\left(\frac{B}{B_0}\right) + \left[ (1 - c) - \left(\frac{B_{\text{cr}}}{B}\right)^{1/2} \right] \quad (31)$$

where  $c$  and  $B_0$  are fitting parameters.

Analyzing the MR of the fabricated SFMO-SMO core-shell structures<sup>[76]</sup> in terms of Serrate's tunneling model,<sup>[73]</sup> we obtain a sufficient fit (**Figure 5**). Here, the magnetic-field parameter  $B_{\text{cr}}$  in the order of 1 mT slows down quadratically with temperature.

We have developed a more complex model for intergranular MR of SFMO ceramics caused by spin-dependent tunneling.<sup>[77]</sup> The resistivity  $\rho$  of a granular metal network in which the metal grains are interconnected by insulating barriers is given by Equation (10) where  $U_c$  is negligible. The tunnel resistance decreases when the magnetic moments of the grains are aligned in parallel to an applied magnetic field. If the angle between the magnetizations on both sides of the tunneling barrier is randomly distributed between 0 and  $\pi$ , the resistivity is given by Equation (13). Taking into account small changes of the barrier height by the applied magnetic field, this yields an MR of

$$\text{MR} = \frac{\rho(B)}{\rho(0)} - 1 = \frac{(1 + m(0, T)^2 \cdot P^2) \cdot \exp(f\chi(0) \cdot w \cdot \frac{\delta V_0}{2V_0})}{(1 + m(B, T)^2 \cdot P^2)} - 1 \quad (32)$$

where  $\rho(B)$  is the resistivity for a given magnetic flux density  $B$  and  $\rho(0)$  is the value of the resistivity for  $B = 0$ . For very large barrier heights ( $\Phi \rightarrow \infty$ ) and very soft magnetic materials (with a coercive field  $B_c \rightarrow 0$ ), we obtain the well-known relation of Equation (29). In the latter model, the maximum MR is  $-50\%$ .

The model parameters were derived as follows.<sup>[77]</sup> Approaching the Curie temperature  $T_C$ , the  $m^2$  changes as  $(T_C - T)/T_C$ . Therefore, we approximate this value by a series expansion

$$m^2(T) = \sum_i a_i \left( \frac{T_C - T}{T_C} \right)^i \quad (33)$$

where  $i = 1, 2, 3, \dots$ . The coefficients of this expansion are slightly different for powders and ceramics (**Table 2**).

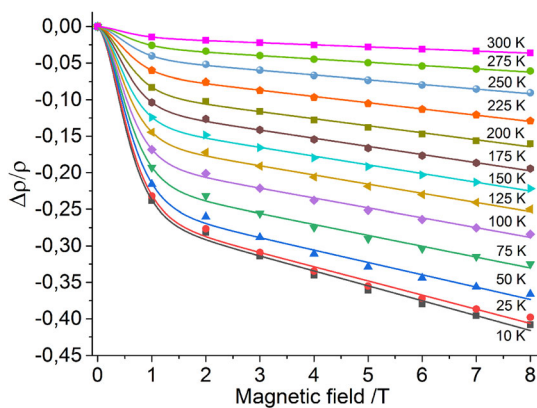


**Figure 5.** Magnetoresistance (MR) of  $\text{Sr}_2\text{FeMoO}_{6-\delta}\text{-SrMoO}_4$  core-shell structures<sup>[76]</sup> fitted to the spin-dependent tunneling model.<sup>[73]</sup>

**Table 2.** Coefficients of the series expansion, Equation (33).

Parameter	Powder	Ceramics
$a_1$	2.04	1.89
$a_2$	-5.32	-1.97
$a_3$	7.19	2.2
$a_4$	-2.89	1.14

The magnetic flux density dependence of the reduced magnetization was modeled by means of a traditional analysis of the approach of magnetization to saturation<sup>[78,79]</sup>

$$m(B) = 1 - \sum_i \left( \frac{\alpha_{i/2}}{B} \right)^{i/2} \quad (34)$$

where each of the lower terms of this expansion is associated with a certain source of magnetic inhomogeneities.  $i$  equals 1, 2, 3 for point, linear, and layered sources, respectively. In contrast, the coefficient  $a_{1/2}$  in SFMO ceramics was related also to the spin-glass-like behavior of grain boundaries,<sup>[73]</sup> which are absent in powder samples. The quadratic terms ( $i = 4$ ) is related to the magnetocrystalline<sup>[80,81]</sup> or shape anisotropy<sup>[82]</sup> as well as to mechanical stress,<sup>[83]</sup> the cubic term ( $i = 6$ ) also includes magnetocrystalline anisotropy.<sup>[81]</sup> Equation (34) is valid for magnetic fields exceeding several times the coercive one. For SFMO-SMO core-shell structures, the coercive field at 4.2 K amounts to  $2\mu_0 H_c \approx 24\text{--}28$  mT.<sup>[84]</sup> With increasing temperature, the coercive field decreases.<sup>[85]</sup>

**Table 3** lists the coefficients of Equation (34) for SFMO powders and ceramics. **Figure 6** compares the calculated values for  $m(T)$  and  $m(B)$  with experimental data. Grain boundaries are absent in powders. Consequently, the first coefficient  $\alpha_{1/2}$  is missing.

Tunneling spin polarization and the interface magnetization followed the same temperature dependence.<sup>[89,90]</sup> In the result, the spin polarization resembles the spontaneous magnetization behavior at low temperatures known as Bloch's  $T^{3/2}$  law<sup>[91]</sup>

$$P(T) = P_0(1 - g \cdot T^{3/2}) \quad (35)$$

Here,  $g$  is a fitting parameter which in the case of magnetization is generally larger for the surface than for the bulk<sup>[92]</sup> and which is very sensitive to surface contaminations.<sup>[93]</sup>

Now, we assume that the dependence of  $P$  on ASD is similar to the dependence of the magnetization on the ASD.<sup>[29]</sup> In this case,  $P(\text{ASD})$  is given by

**Table 3.** Coefficients of the series expansion, Equation (34).

Parameter	Powder	Ceramics
$\alpha_{1/2}$ [mT]	–	7.4
$\alpha_1$ [mT]	85	16
$\alpha_2$ [mT]	115	–
$\alpha_3$ [mT]	118	–

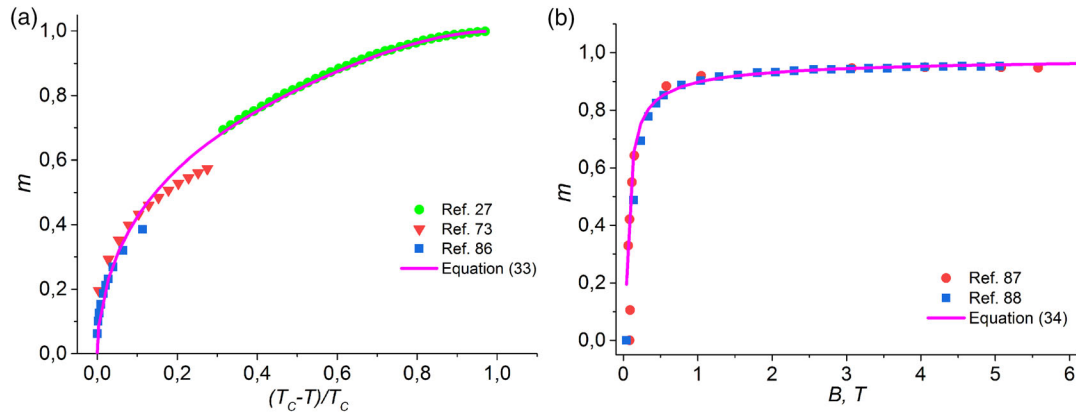


**Figure 6.** Comparison of a) the empirical relationship  $m(T)$ , Equation (33), with experimental data<sup>[27,73,86]</sup> as well as the scaling law of spontaneous polarization for SFMO at  $T < T_C$ <sup>[86]</sup>, and b) of the empirical relationship  $m(B)$ , Equation (34), with experimental data.<sup>[87,88]</sup> Adapted with permission.<sup>[77]</sup> Copyright 2021, Elsevier.

$$P(\text{ASD}) = P_0(1 - 2 \cdot \text{ASD}) \quad (36)$$

**Figure 7** compares the calculated temperature dependence of the MR originating from spin-dependent tunneling with experimental data.<sup>[94]</sup>

The model slightly overestimates the field dependence of the TMR in the low-field region since the coercive field was not accounted. In contrast, there is an increase of the contribution of the conventional MR at higher magnetic fluxes,  $B > 2 \text{ T}$ ,<sup>[95]</sup> which was not included into the present model. Nevertheless, our model applies to the range of about 4–6 T.

### 3.2.2. Intergrain MR in the Presence of a Magnetically Disordered Interface Layer

An additional layer of disordered spins at the interface lowers the term  $m^2 P^2$  to  $m^2 P^2 \langle \cos^2 \varphi' \rangle = 1/3 \cdot m^2 P^2$ . Here,  $\varphi'$  is the angle between the spin orientation in the disordered layer and the magnetization  $M$ .<sup>[61]</sup> Following Equation (15), the

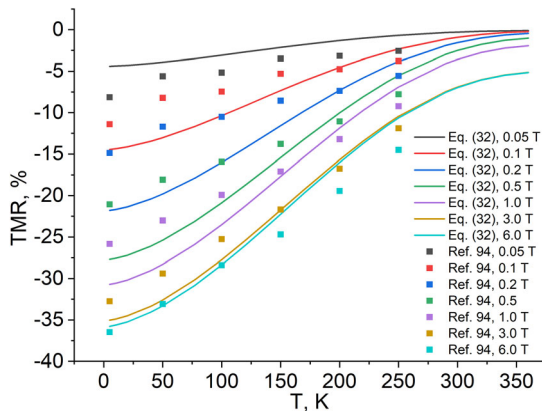


**Figure 7.** Temperature dependence of the MR calculated by means of Equation (32) (solid lines) in comparison with experimental data (squares).<sup>[94]</sup> Adapted with permission.<sup>[77]</sup> Copyright 2021, Elsevier.

MR in the presence of a magnetically disordered interface layer is then given by

$$\text{MR} = \frac{\rho(B)}{\rho(0)} - 1 = \frac{(3 + m(0, T)^2 \cdot P^2) \cdot \exp(f\chi(0) \cdot w \cdot \frac{\delta V_0}{2V_0})}{(3 + m(B, T)^2 \cdot P^2)} - 1 \quad (37)$$

Thus, the maximum MR—for very large barrier heights ( $\Phi \rightarrow \infty$ ) and very soft magnetic materials ( $B_c \rightarrow 0$ )—becomes  $\sim 25\%$ .

### 3.2.3. Intergrain MR Beyond the -Thin-Barrier Limit

Beyond the thin-barrier limit, the MR resulting from the term  $G_{4/3} \cdot T^{4/3}$  in Equation (19) yields

$$\text{MR} \approx \left(1 + \frac{\delta V_0}{2V_0}\right)^{3/2} \cdot \exp\left(\frac{f\chi(0) \cdot w \cdot \delta V_0 / V_0}{6}\right) - 1 \quad (38)$$

This contribution is one order of magnitude smaller than the intergrain MR due to spin-dependent tunneling and, consequently, out of the range for technical applications. Therefore, it will not be considered further in this work.

### 3.2.4. Intergrain MR Due to FIT

With regard to Equation (24), the MR of FIT is given by

$$\text{MR} = \exp\left(\frac{T_1(B)}{T_0(B) + T} - \frac{T_1(0)}{T_0(0) + T}\right) - 1 \quad (39)$$

where the parameters  $T_1(0)$  and  $T_0(0)$  are given by Equations (21) and (23), respectively, while  $T_1(B)$  and  $T_0(B)$  are defined by the magnetic-field dependence, Equation (25).

The predicted temperature dependence of the MR in nano-sized, granular SFMO-SMO core-shell structure (**Figure 8**) is much weaker than in the SFMO ceramics. This weak temperature dependence would be an advantage for device applications near room temperature. It is a consequence of the parameter  $T_0$

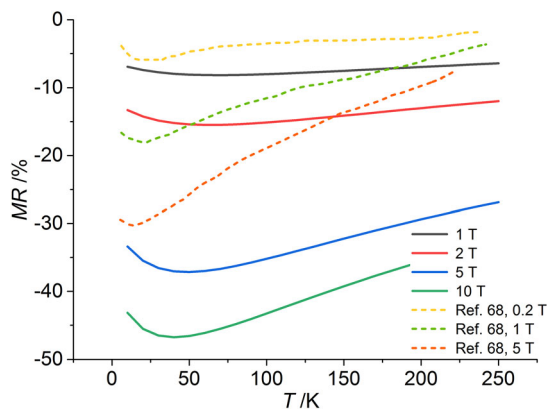


**Figure 8.** Calculated temperature dependence of the magnetoresistance of nanosized, granular SFMO-SMO core-shell structures with magnetic flux density as parameter in comparison with experimental data of granular SFMO ceramics.<sup>[68]</sup> Adapted with permission.<sup>[44]</sup> Copyright 2021, Wiley-VCH.

in the order of the temperature at resistivity measurements. The increase of the MR at low temperatures followed by a decrease is in qualitative accordance with experimental data for granular SFMO samples attributed to the FIT model.<sup>[68]</sup>

#### 4. Conclusions

The electrical conductivity and, correspondingly, the magnetoresistivity of strontium ferromolybdate ceramics depend significantly on the conditions at grain boundaries. With increasing thickness of the intergrain tunneling barrier, the mechanism of intergrain conductivity evolves from pure spin-dependent tunneling via the appearance of hopping transport through defect-induced localized states up to FIT at nanosized tunneling contacts. As a result, a wider and defective intergrain tunneling barrier deteriorates the magnetoresistance. Additionally, the magnetoresistance diminishes in the presence of a magnetically disordered interface layer. These findings are fundamental for the manufacture of magnetic sensors based on core-shell structures.

#### Supporting Information

Supporting Information is available from the Wiley Online Library or from the author.

#### Acknowledgements

This work was developed within the scope of the European project H2020-MSCA-RISE-2017-778308-SPINMULTIFILM.

Open Access funding enabled and organized by Projekt DEAL.

#### Conflict of Interest

The authors declare no conflict of interest.

#### Data Availability Statement

Data sharing is not applicable to this article as no new data were created or analyzed in this study.

#### Keywords

magnetoresistance, resistivity, spin-dependent tunneling, strontium ferromolybdate

Received: January 12, 2022

Revised: May 12, 2022

Published online:

- [1] W. Thomson, *Proc. R. Soc. London* **1857**, *8*, 546.
- [2] M. N. Baibich, J. M. Broto, A. Fert, F. N. Van Dau, F. Petroff, P. Eitenne, G. Creuzet, A. Friederich, J. Chazelas, *Phys. Rev. Lett.* **1988**, *61*, 2472.
- [3] G. Binasch, P. Grünberg, F. Saurenbach, W. Zinn, *Phys. Rev. B* **1989**, *39*, 4828(R).
- [4] A. E. Berkowitz, J. R. Mitchell, M. J. Carey, A. P. Young, S. Zhang, F. E. Spada, F. T. Parker, A. Hutten, G. Thomas, *Phys. Rev. Lett.* **1992**, *68*, 3745.
- [5] J. Q. Xiao, J. S. Jiang, C. L. Chien, *Phys. Rev. Lett.* **1992**, *68*, 3749.
- [6] M. Julliere, *Phys. Lett. A* **1975**, *54A*, 225.
- [7] G. H. Jonker, J. H. Van Santen, *Physica* **1950**, *16*, 337.
- [8] A. P. Ramirez, *J. Phys.: Condens. Matter* **1997**, *9*, 8171.
- [9] S. A. Solin, T. Thio, D. R. Hines, J. J. Heremans, *Science* **2000**, *289*, 1530.
- [10] J. Suh, W. Kim, J. Chang, S.-H. Han, E. Kim, *J. Korean Phys. Soc.* **2009**, *55*, 577.
- [11] M. Rajeswari, C. H. Chen, A. Goyal, C. Kwon, M. C. Robson, R. Ramesh, T. Venkatesan, *Appl. Phys. Lett.* **1996**, *68*, 3555.
- [12] W. Eerenstein, T. T. M. Palstra, S. S. Saxena, T. Hibma, *Phys. Rev. Lett.* **2002**, *88*, 4.
- [13] A. Nag, S. Jana, S. Middey, S. Ray, *IOP Conf. Ser.: Mater. Sci. Eng.* **2013**, *46*, 012001.
- [14] A. Venimadhav, F. Sher, J. P. Attfield, M. G. Blamire, *J. Magn. Magn. Mater.* **2004**, *269*, 101.
- [15] J. Zhang, W. J. Ji, J. Xu, X. Y. Geng, J. Zhou, Z. Bin Gu, S. H. Yao, S. T. Zhang, *Sci. Adv.* **2017**, *3*, e1701473.
- [16] C. N. R. Rao, *Philos. Trans. R. Soc. London. Ser. A: Math. Phys. Eng. Sci.* **1998**, *356*, 23.
- [17] X. M. Feng, G. H. Rao, G. Y. Liu, W. F. Liu, Z. W. Ouyang, J. K. Liang, *J. Phys.: Condens. Matter* **2004**, *16*, 1813.
- [18] G. Y. Liu, G. H. Rao, X. M. Feng, H. F. Yang, Z. W. Ouyang, W. F. Liu, J. K. Liang, *Physica B* **2003**, *334*, 408.
- [19] D. Niebieskikwiat, R. Sánchez, A. Caneiro, L. Morales, M. Vásquez-Mansilla, F. Rivadulla, L. Hueso, *Phys. Rev. B* **2000**, *62*, 3340.
- [20] J. S. Moodera, L. R. Kinder, T. M. Wong, R. Meservey, *Phys. Rev. Lett.* **1995**, *74*, 3273.
- [21] T. Miyazaki, N. Tezuka, *J. Magn. Magn. Mater.* **1995**, *139*, L231.
- [22] W. H. Butler, X. G. Zhang, T. C. Schulthess, J. M. MacLaren, *Phys. Rev. B* **2001**, *63*, 054416.
- [23] J. Mathon, A. Umerski, *Phys. Rev. B* **2001**, *63*, 220403(R).
- [24] S. Ikeda, J. Hayakawa, Y. Ashizawa, Y. M. Lee, K. Miura, H. Hasegawa, M. Tsunoda, F. Matsukura, H. Ohno, *Appl. Phys. Lett.* **2008**, *93*, 082508.
- [25] J. Paul, C. Schnieders, J. Traute, A. Conca, B. Leven, B. Hillebrands, presented at *13th Symp. Magnetoresistive sensors and magnetic systems*, Wetzlar, Germany, March **2015**.

- [26] H. Y. Hwang, S.-W. Cheong, N. P. Ong, B. Batlogg, *Phys. Rev. Lett.* **1996**, *77*, 2041.
- [27] K. I. Kobayashi, T. Kimura, H. Sawada, K. Terakura, Y. Tokura, *Nature* **1998**, *395*, 677.
- [28] Y. C. Hu, J. J. Ge, Q. Ji, B. Lv, X. S. Wua, G. F. Cheng, *Powder Diffr.* **2010**, *25*, S17.
- [29] L. Balcells, J. Navarro, M. Bibes, A. Roig, B. Martínez, J. Fontcuberta, *Appl. Phys. Lett.* **2001**, *78*, 781.
- [30] B. J. Park, H. Han, J. Kim, Y. J. Kim, C. S. Kim, B. W. Lee, *J. Magn. Magn. Mater.* **2004**, *272*, 1851.
- [31] L. Harnagea, P. Berthet, *J. Solid State Chem.* **2015**, *222*, 115.
- [32] Y. Tomioka, T. Okuda, Y. Okimoto, R. Kumai, K. Kobayashi, Y. Tokura, *Phys. Rev. B* **2000**, *61*, 422.
- [33] Y. Moritomo, S. Xu, A. Machida, T. Akimoto, E. Nishibori, M. Takata, M. Sakata, K. Ohoyama, *J. Phys. Soc. Jpn.* **2000**, *69*, 1723.
- [34] H. Yanagihara, M. B. Salamon, Y. Lyanda-Geller, S. Xu, Y. Moritomo, *Phys. Rev. B* **2001**, *64*, 214407.
- [35] O. Erten, O. N. Meetei, A. Mukherjee, M. Randeria, N. Trivedi, P. Woodward, *Phys. Rev. B* **2013**, *87*, 165105.
- [36] J. Ziman, *Electrons and Phonons*, Clarendon Press, Oxford **1960**.
- [37] I. Mannari, *Prog. Theor. Phys.* **1959**, *22*, 335.
- [38] W. Westerburg, D. Reisinger, G. Jakob, *Phys. Rev. B* **2000**, *62*, R767.
- [39] K. Kubo, N. Ohatata, *J. Phys. Soc. Jpn.* **1972**, *33*, 21.
- [40] D. D. Sarma, P. Mahadevan, T. Saha-Dasgupta, S. Ray, A. Kumar, *Phys. Rev. Lett.* **2000**, *85*, 2549.
- [41] M. Jaime, P. Lin, M. Salamon, P. Han, *Phys. Rev. B* **1998**, *58*, R5901.
- [42] G. Li, H. D. Zhou, S. J. Feng, X. J. Fan, X. G. Li, Z. D. Wang, *J. Appl. Phys.* **2002**, *92*, 1406.
- [43] F. J. Dyson, *Phys. Rev.* **1956**, *102*, 1217.
- [44] G. Suchanek, E. Artukh, *Phys. Status Solidi B* **2021**, *258*, 2000629.
- [45] Z. Shining, Z. Xingkuai, X. Ziran, W. Hao, X. Hua, *Chin. Phys. Lett.* **1989**, *6*, 185.
- [46] N. Kalanda, V. Turchenko, D. Karpinsky, S. Demyanov, M. Yarmolich, M. Balasoiu, N. Lupu, S. Tyutyunnikov, N. A. Sobolev, *Phys. Status Solidi B* **2019**, *256*, 1800278.
- [47] W. Westerburg, Ph.D. Thesis, Universität Mainz **2000**.
- [48] M. Besse, V. Cros, A. Barthélémy, H. Jaffrès, J. Vogel, F. Petroff, A. Mirone, A. Tagliaferri, P. Bencok, P. Decorse, P. Berthet, Z. Szotek, W. M. Temmerman, S. S. Dhesi, N. B. Brookes, A. Rogalev, A. Fert, *Europhys. Lett.* **2002**, *60*, 608.
- [49] D. Phuyal, S. Mukherjee, S. K. Panda, G. J. Man, K. Simonov, L. Simonelli, S. M. Butorin, H. Rensmo, O. Karis, *J. Phys. Chem. C* **2021**, *125*, 11249.
- [50] J. S. Helman, B. Abeles, *Phys. Rev. Lett.* **1976**, *37*, 1429.
- [51] Y. Xu, D. Ephron, M. R. Beasley, *Phys. Rev. B* **1995**, *52*, 2843.
- [52] B. Abeles, P. Sheng, M. D. Coutts, Y. Arie, *Adv. Phys.* **1975**, *24*, 407.
- [53] G. Suchanek, N. Kalanda, E. Artukh, M. Yarmolich, N. A. Sobolev, *J. Alloys Compd.* **2021**, *860*, 158526.
- [54] K. Wang, Y. Sui, *Solid State Commun.* **2004**, *129*, 135.
- [55] J. J. Alvarado-Flores, R. Mondragón-Sánchez, M. L. Ávalos-Rodríguez, J. V. Alcaraz-Vera, J. G. Rutiaga-Quiñones, S. J. Guevara-Martínez, *Int. J. Hydrogen Energy* **2021**, *46*, 26185.
- [56] J. G. Simmons, *J. Appl. Phys.* **1963**, *34*, 1793.
- [57] J. Inoue, S. Maekawa, *Phys. Rev. B* **1996**, *53*, R11927.
- [58] P. Sheng, B. Abeles, Y. Arie, *Phys. Rev. Lett.* **1973**, *31*, 44.
- [59] S. Mitani, S. Takahashi, K. Takashi, K. Yakushiji, S. Maekawa, H. Fujimori, *Phys. Rev. Lett.* **1998**, *81*, 2799.
- [60] L. D. Hien, N. P. Duong, L. N. Anh, T. T. Loan, S. Soontaranon, A. de Visser, *J. Alloys Compd.* **2019**, *793*, 375.
- [61] S. Lee, H. Y. Hwang, B. I. Shraiman, W. D. Ratcliff, S.-W. Cheong, *Phys. Rev. Lett.* **1999**, *82*, 4508.
- [62] For parallel conduction channels, the overall conductance is the sum of the individual conductances.
- [63] N. G. Van Kampen, *Physica* **1960**, *26*, 585.
- [64] P. Sheng, E. K. Sichel, J. I. Gittleman, *Phys. Rev. Lett.* **1978**, *40*, 1197.
- [65] B. Fisher, B. Chashka, L. Patlagan, M. Reisner, *Phys. Rev. B* **2003**, *68*, 1.
- [66] B. Fisher, K. B. Chashka, L. Patlagan, G. M. Reisner, *Curr. Appl. Phys.* **2004**, *4*, 518.
- [67] B. Fisher, J. Genossar, K. B. Chashka, L. Patlagan, G. M. Reisner, *Solid State Commun.* **2006**, *137*, 641.
- [68] B. Fisher, K. B. Chashka, L. Patlagan, G. M. Reisner, *J. Magn. Magn. Mater.* **2004**, *272–276*, 1790.
- [69] B. Fisher, J. Genossar, K. B. Chashka, L. Patlagan, G. M. Reisner, *EPJ Web Conf.* **2014**, *75*, 01001.
- [70] L. López-Mir, C. Frontera, H. Aramberri, K. Bouzehouane, J. Cisneros-Fernández, B. Bozzo, L. Balcells, B. Martínez, *Sci. Rep.* **2018**, *8*, 861.
- [71] O. Erten, O. N. Meetei, A. Mukherjee, M. Randeria, N. Trivedi, P. Woodward, *Phys. Rev. Lett.* **2011**, *107*, 257201.
- [72] B. I. Shklovskii, A. L. Efros, *Zh. Eksp. Teor. Fiz.* **1983**, *84*, 811 [*Sov. Phys. JETP* **1983**, *57*, 470].
- [73] D. Serrate, J. M. De Teresa, P. A. Algarabel, M. R. Ibarra, J. Galibert, *Phys. Rev. B* **2005**, *71*, 104409.
- [74] E. K. Hemery, G. V. M. Williams, H. J. Trodahl, *Physica B* **2007**, *390*, 175.
- [75] C. L. Chien, *Annu. Rev. Mater. Sci.* **1995**, *25*, 129.
- [76] N. Kalanda, M. Yarmolich, S. Demyanov, A. Petrov, V. M. Garamus, H. Terryn, J. Ustarroz, N. A. Sobolev, in *Fundamental and Applied Nano-Electromagnetics II*, NATO Science for Peace and Security Series B: Physics and Biophysics (Eds: A. Maffucci, S. Maksimenko), Springer, Dordrecht, Netherlands **2019**, pp. 21–40.
- [77] E. Artukh, G. Suchanek, *Open Ceram.* **2021**, *7*, 100171.
- [78] W. F. Brown, *Phys. Rev.* **1940**, *58*, 736.
- [79] W. F. Brown, *Micromagnetics*, 1st ed., Wiley, New York **1963**.
- [80] N. S. Akulov, *Zeitschrift für Phys.* **1931**, *69*, 822.
- [81] R. Grössinger, *Phys. Status Solidi A* **1981**, *66*, 665.
- [82] T. Holstein, H. Primakoff, *Phys. Rev.* **1941**, *59*, 388.
- [83] R. Gans, *Ann. Phys.* **1932**, *407*, 28.
- [84] N. Kalanda, V. Garamus, M. Avdeev, M. Zheludkevich, M. Yarmolich, M. Serdechnova, D. C. Florian Wieland, A. Petrov, A. Zhaludkevich, N. Sobolev, *Phys. Status Solidi B* **2019**, *256*, 1800428.
- [85] I. Angervo, M. Saloaro, H. Palonen, S. Majumdar, H. Huhtinen, P. Paturi, *Phys. Proc* **2015**, *75*, 1011.
- [86] H. Yanagihara, W. Cheong, M. B. Salamon, S. Xu, Y. Moritomo, *Phys. Rev. B* **2002**, *65*, 092411.
- [87] J. Navarro, J. Nogués, J. S. Muñoz, J. Fontcuberta, *Phys. Rev. B* **2003**, *67*, 174416.
- [88] R. Kirchheisen, J. Töpfer, *J. Solid State Chem.* **2012**, *185*, 76.
- [89] J. S. Moodera, J. Nowak, R. J. M. Van De Veerdonk, *Phys. Rev. Lett.* **1998**, *80*, 2941.
- [90] A. H. Mac Donald, T. Jungwirth, M. Kasner, *Phys. Rev. Lett.* **1998**, *81*, 705.
- [91] C. H. Shang, J. Nowak, R. Jansen, J. S. Moodera, *Phys. Rev. B* **1998**, *58*, R2917.
- [92] D. T. Pierce, R. J. Celotta, J. Unguris, H. C. Siegmans, *Phys. Rev. B* **1982**, *26*, 2566.
- [93] D. Mauri, D. Scholl, H. C. Siegmans, E. Kay, *Phys. Rev. Lett.* **1988**, *61*, 758.
- [94] D. Niebieskikwiat, A. Caneiro, R. D. Sánchez, J. Fontcuberta, *Phys. Rev. B* **2001**, *64*, 180406.
- [95] M. Venkatesan, C. B. Fitzgerald, U. V. Varadaraju, J. M. D. Coey, *IEEE Trans. Magn.* **2002**, *38*, 2901.